Journal of Power Sources 266 (2014) 114–120

Contents lists available at ScienceDirect

Journal of Power Sources

journal homepage: www.elsevier.com/locate/jpowsour

Solid-state synthesis of submicron-sized $Li_4Ti_5O_{12}/Li_2TiO_3$ composites with rich grain boundaries for lithium ion batteries

Ying Wang, Aijun Zhou, Xinyi Dai, Lidong Feng, Jianwen Li, Jingze Li*

State Key Laboratory of Electronic Thin Films and Integrated Devices, School of Microelectronics and Solid-State Electronics, University of Electronic Science and Technology of China, Chengdu 610054, China

HIGHLIGHTS

- Submicron-sized $Li_4Ti_5O_{12}/Li_2TiO_3$ was synthesized by solid state process.
- $Li_4Ti_5O_{12}/Li_2TiO_3$ composite exhibited excellent rate performance.
- $Li_4Ti_5O_{12}/Li_2TiO_3$ composite demonstrated outstanding cycle stability.
- The ionic conductivity of $Li_4Ti_5O_{12}/Li_2TiO_3$ was higher than that of $Li_4Ti_5O_{12}$.

ARTICLE INFO

Article history:
Received 5 February 2014
Received in revised form
1 May 2014
Accepted 5 May 2014
Available online 14 May 2014

Keywords:
Grain boundary
$Li_4Ti_5O_{12}/Li_2TiO_3$
$Li_4Ti_5O_{12}$
Anode
Lithium ion battery

ABSTRACT

Submicron-sized $Li_4Ti_5O_{12}/Li_2TiO_3$ composites with Li-rich grain boundaries are successfully synthesized by a simple, environmentally benign, mass production preferred solid state process. The crystal phase and morphology are characterized by XRD and SEM. The electrochemical performance is collected by galvanostatic discharge–charge tests, cyclic voltammograms (CV) and electrochemical impedance spectra (EIS) tests. The initial discharge capacity of $Li_4Ti_5O_{12}/Li_2TiO_3$ composite is 155 mAh g^{-1} at 0.5 C. While the current rate is as high as 10 C, the specific capacity is 113 mAh g^{-1}, and the capacity retention is 98.2% even after 500 cycles. As a reference, the ionic conductivity and the electrochemical performance of Li_2TiO_3 and $Li_4Ti_5O_{12}/TiO_2$ composite are also characterized. The extraordinary high rate performance and cycling stability are explained by high ionic conductivity and rich grain boundaries of $Li_4Ti_5O_{12}/Li_2TiO_3$ composite.

1. Introduction

With increasing energy crisis and alarming environmental problems aroused by fossil fuels consuming, batteries are intensively studied as the largest group of technologies and the most convenient device to store electrical energy generated by alternative energy sources (solar, wind, and tide energy, etc.) [1]. Lithium ion batteries have been commercialized for mobile phones and laptop computers due to their high energy density. Recently, lithium ion batteries have been widely expected to drive electric vehicles (EVs) and hybrid electric vehicles (HEVs) [2,3], and have high value opportunity to be applied to electrical energy storage for the grid [4–6]. Anode is one of the most important part of a battery. Considering carbon based anodes, the low operating potential of 100 mV (vs. Li/Li^+) tends to induce the growth of lithium dendrites at high charge/discharge rates, which will make a short circuit possible [7]. Alternative anode materials of silicon and tin have been extensively studied for their attractive specific capacities [8]. However, the poor cycle stability caused by immense volume expansion in the process of lithiation stands in the way of commercialization. In spite of less competitive specific energy density relative to carbon, tin, and silicon-based materials, spinel lithium titanate ($Li_4Ti_5O_{12}$) is considered as one of the most promising anodes for its higher discharge/charge plateau (about 1.55 V vs. Li/Li^+) and zero strain characteristic which can provide possible solutions to the challenges of safety and cycle stability for advanced batteries [9–11]. Evidently, it is the poor rate performance resulted from quite low electronic conductivity ($<10^{-13}$ S cm^{-1}) [12] and intermediate Li^+ ion conductivity of pristine $Li_4Ti_5O_{12}$ that retards it from commercialization.

* Corresponding author. No. 4, Section 2, North Jianshe Road, Chengdu, Sichuan 610054, China. Tel.: +86 28 83207620; fax: +86 28 83202569.
E-mail addresses: wangyingwl@163.com (Y. Wang), zhouaj@uestc.edu.cn (A. Zhou), daixinyi20062008@126.com (X. Dai), Fld198812@163.com (L. Feng), 523200835@qq.com (J. Li), lijingze@uestc.edu.cn (J. Li).

http://dx.doi.org/10.1016/j.jpowsour.2014.05.002
0378-7753/

Traditional methods for improving electronic conductivity and ionic conductivity mainly focus on cation doping (Mg, Al, V, etc. [12–16]), surface modification (carbon, polyacene, etc. [17–22]), and size control [23,24]. More recently, composites of $Li_4Ti_5O_{12}$/Ag [25–28], $Li_4Ti_5O_{12}$/Au [29], $Li_4Ti_5O_{12}$/Cu [30,31], and $Li_4Ti_5O_{12}$/CNT [32] have been widely investigated to improve particle-to-particle and particle-to-current collector electric contact. Alternatively, nanocomposites of $Li_4Ti_5O_{12}$ and metal oxides can provide rich grain boundaries with high concentration of diffusion-mediating defects, which make fast diffusivity possible. In this regarding, dual-phase $Li_4Ti_5O_{12}$–TiO_2 has been synthesized with improved rate capability [33–35]. According to pseudo-binary Li_2O–TiO_2 phase diagram [36] depicted in Kleykamp's work, it is easy to get $Li_4Ti_5O_{12}/Li_2TiO_3$ composite under 930 °C when the molar ratio of TiO_2 is less than 71.4%, which has been demonstrated experimentally by Fray's team [37]. To the best of our knowledge, there is no report considering the compact of Li_2TiO_3 on the electrochemical performance of $Li_4Ti_5O_{12}$.

In this work, $Li_4Ti_5O_{12}/Li_2TiO_3$ composites were successfully synthesized by a simple solid state process. As the references, $Li_4Ti_5O_{12}/TiO_2$ composites and pristine $Li_4Ti_5O_{12}$ were similarly prepared by varying the molar ratio of Li:Ti. $Li_4Ti_5O_{12}/Li_2TiO_3$ composite with Li:Ti molar ratio of 4.8:5 showed the best rate performance and outstanding cyclic stability, which might be attributed to the improved ion transport property and the unique structure of the Li-rich composite. Li^+ ion conductivity of $Li_4Ti_5O_{12}/Li_2TiO_3$ composite was 1.7×10^{-6} S cm^{-1}, which was much higher than that of pristine $Li_4Ti_5O_{12}$ (5.7×10^{-7} S cm^{-1}), Li_2TiO_3 (2.5×10^{-7} S cm^{-1}), and $Li_4Ti_5O_{12}/TiO_2$ nanocomposite (4.2×10^{-7} S cm^{-1}). A Li-rich interphase layer formed between $Li_4Ti_5O_{12}$ and Li_2TiO_3 might be helpful to stabilize the crystal structure of the active material, resulting in enhanced cyclic stability.

2. Experimental

2.1. Material preparation

TiO_2 (anatase, AR) and Li_2CO_3 (industrial grade) were used as the starting materials. The precursors were prepared by mixing TiO_2 and Li_2CO_3 powder with the aid of ethanol in a planetary ball mill for 4 h at a speed of 400 r min^{-1}. The ball feed ratio was set at 5:1. After ball-milling, the slurries were then transferred to a dry box and dried at 80 °C. The dried products were milled for the solid state reaction process. The sintering procedure in the tube furnace was set as follows: heating from room temperature to 750 °C at a rate of 2 °C min^{-1}, holding at the maximum temperature for 12 h, then cooling down naturally. The whole process was carried out in air. To optimize the electrode performance, Li:Ti ratios ranging from 4:6, 4:5.5, 4:5, 4.2:5, 4.4:5, 4.8:5, 5.2:5, 5.6:5 to 10:5 were investigated. The samples were named T2, T1, T0, L0, L1, L2, L3, L4 and Li_2TiO_3, respectively. For ionic conductivity testing, the as-synthesized powders (0.25 g) were compressed into small platelets (ϕ = 1.3 cm) under the pressure of 60 KN, then the prepared platelets were sealed in the lab cell cases for the characterization.

2.2. Material characterization

XRD diffraction (XRD, x'pert pro MPD, Cu Kα radiation) was employed to collect crystalline phase data in the scanning range (2θ) of 10°–85° at a step size of 0.03° min^{-1}. A field emission scanning electron microscopy (FESEM, Hitachi S-4800) was employed to get morphology information of the samples. To determine the tap density, the powder (2 g) was placed into a graduated cylinder (10 ml), which was then tapped 300 times on a lab bench by hand.

2.3. Battery assembly

Battery tests were based on two-electrode half cells. The active materials and acetylene black were grinded in a carnelian mortar by hand to ensure finer powder and a compact mixing. Further grinding was needed after the solution of polyvinylidene (PVDF) dissolved in *N*-methyle-2-pyrrolidine (NMP) was added. The weight ratio of active material, acetylene black, and binder was 80:10:10. Then the mixed slurry was deposited on a thin copper foil by a doctor blade process and dried at 80 °C for 5–6 h afterward. The covered copper foil was finally punched into round pieces with a diameter of 1 cm (average mass loading ≥1.7 mg cm^{-2}). The as-prepared electrodes were stored in a vacuum oven for further drying of another 12 h before they were transferred into a glove box for battery assembly. The glove box was circulated with argon gas (99.99%) to ensure a clear atmosphere (O_2 < 5 ppm, H_2O < 5 ppm). The counter electrode used in the half cell was lithium foil. 1 M $LiPF_6$ in ethylene carbonate (EC)-diethyl carbonate (DEC) (1:1 in volume) was chosen as the electrolyte.

2.4. Battery test

A LAND series battery testing system (CT2001A/CT2001C; Wuhan Kinguo Electronics Co., Ltd.) was employed to conduct galvanostatic discharge–charge tests. The potential range was set at 3.0–1.0 V. The discharge–charge rates were set to 0.5 C, 1 C, 2 C, 5 C, and 10 C, respectively. An electrochemical analyzer (Solartron Model 1287/1260A; Solartron Analytical) was employed to collect CV curves and electrochemical impedance spectroscopy (EIS)

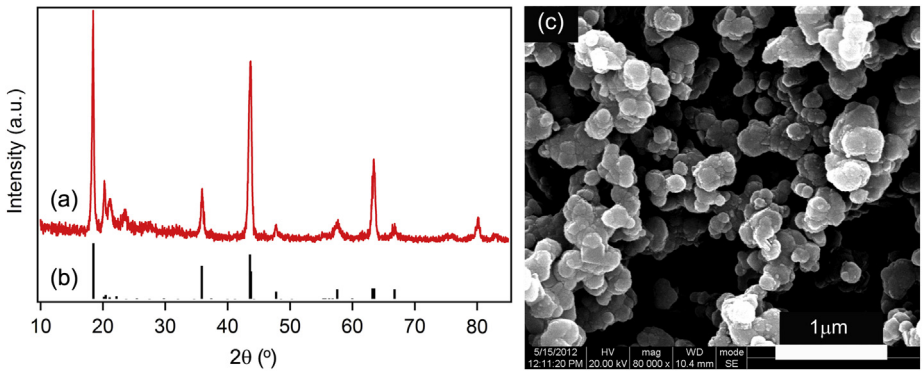

Fig. 1. The structure and morphology of Li_2TiO_3 (a) XRD patterns of the as-prepared Li_2TiO_3 (b) Li_2TiO_3, PDF#33-0831 (c) SEM images of Li_2TiO_3.

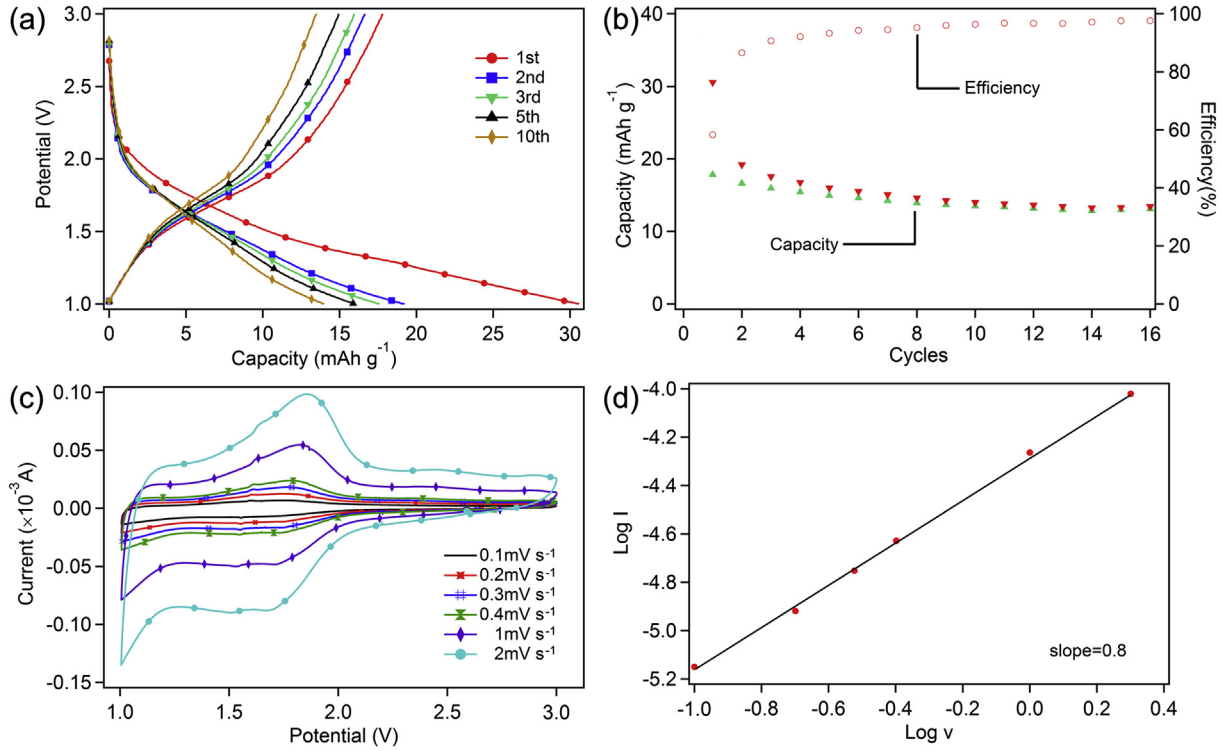

Fig. 2. The electrochemical performance of Li_2TiO_3 (a) the galvanostatic discharge–charge curves (b) the efficiency of the first 16 cycles (c) the cyclic voltammograms at different scan rates (d) the relationship between the peak current and scan rates.

information. CV data was recorded with different scan rates of 0.1 mV s^{-1}, 0.2 mV s^{-1}, 0.3 mV s^{-1}, 0.4 mV s^{-1}, 1 mV s^{-1}, and 2 mV s^{-1} with a potential range of 1.0–3.0 V. EIS spectra were obtained in the frequency range of 0.1 Hz–1 MHz, where the DC potential was 1.55 V for all batteries.

2.5. Ionic conductivity test

EIS of the active material platelet was tested using AC oscillation amplitude of 10 mV with the frequency ranging from 1 Hz to 1 MHz. The ionic conductivity was determined by the formula $\sigma = d/R_bS$, where σ is the ionic conductivity, d, S, R_b are thickness, area and resistance of the platelet, respectively.

3. Results and discussion

3.1. Structure and morphology characterization and electrochemical performance of Li_2TiO_3

XRD pattern of Li_2TiO_3 presented in Fig. 1(a) is consistent with a C2/c (15) (PDF#33-0831) (shown in Fig. 1(b)) structure, whose cell parameters are $a = 5.069$ Å, $b = 8.799$ Å, $c = 9.759$ Å, respectively. This result agrees with the report by Kleykamp [36] and can be assigned to a low-temperature β-phase monoclinic structure. Fig. 1(c) shows SEM image of the as-synthesized Li_2TiO_3, where the distribution of the particle size is from few 10 nm to few hundred nanometers. Closely checking the morphologies of the large

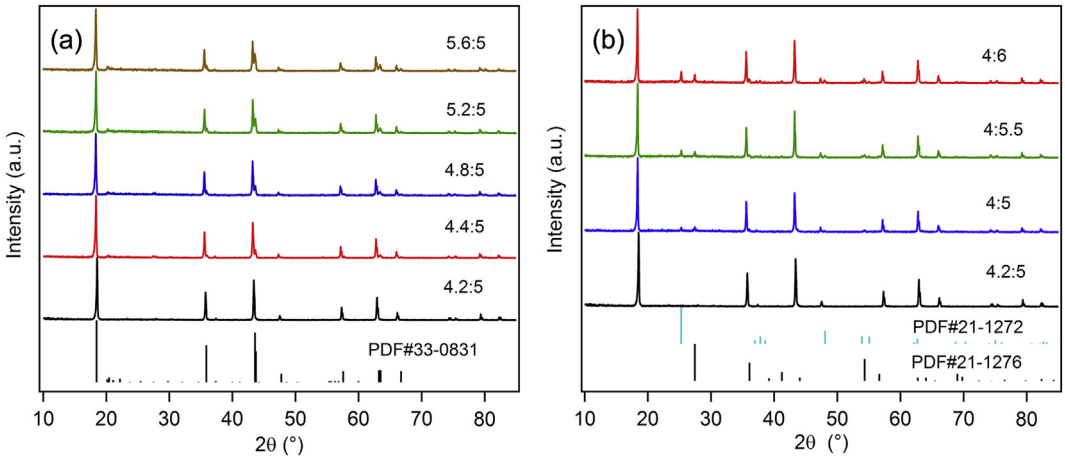

Fig. 3. XRD patterns of the samples synthesized with different Li:Ti ratios. (a) $Li_4Ti_5O_{12}/Li_2TiO_3$ composites (L1 – 4.4:5, L2 – 4.8:5, L3 – 5.2:5, L4 – 5.6:5) and pure $Li_4Ti_5O_{12}$ (L0 – 4.2:5) (b) $Li_4Ti_5O_{12}/TiO_2$ composites (T2 – 4:6, T1 – 4:5.5, T0 – 4:5) and pure $Li_4Ti_5O_{12}$ (L0 – 4.2:5).

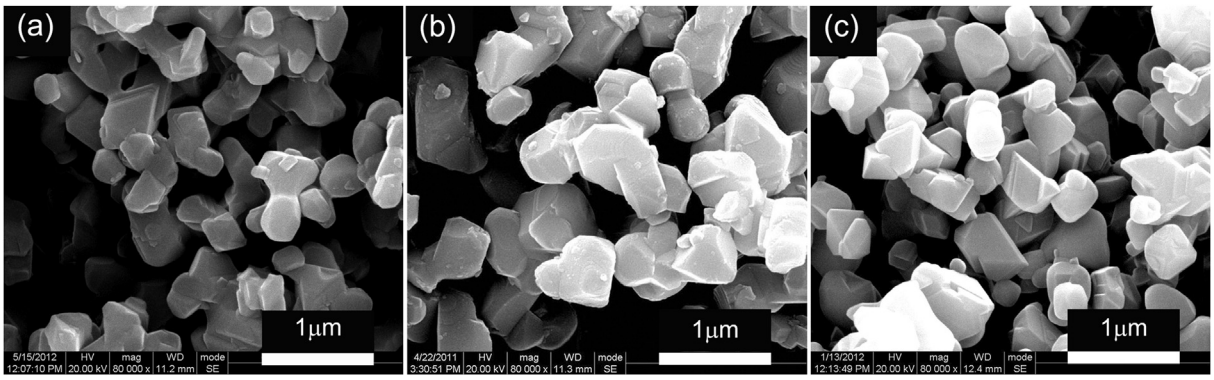

Fig. 4. SEM images of the as-prepared samples. (a) $Li_4Ti_5O_{12}/TiO_2$ composite T1 (b) pure $Li_4Ti_5O_{12}$ (c) $Li_4Ti_5O_{12}/Li_2TiO_3$ material L2.

particles, it seems each large particle is the aggregation of small nanoparticles. Hence, the broadening of XRD peaks can be ascribed to these nanostructured particles.

The electrochemical performance of Li_2TiO_3 is displayed in Fig. 2. Checking the galvanostatic discharge–charge curves at a current rate of 0.5 C (shown in Fig. 2(a)) and the coulombic efficiency data (shown in Fig. 2(b)), three main features can be concluded. First of all, the specific discharge capacity in the first cycle is 30 mAh g^{-1}, which is between the capacity of lower than 10 mAh g^{-1} reported by Tabuchi [38] and the value of 47 mAh g^{-1} reported by Morales [39]. The discrepancy can be ascribed to different particle sizes induced by different synthesis processes employed in the sample preparation or different discharge–charge rates used. No obvious plateau can be observed from the curves, which can be understood that non-faradic phenomenon dominates over the discharge and charge processes rather than the electrochemical redox reaction at a discharge–charge rate of 0.5 C. Secondly, large capacity loss in the first cycle and a less rapid but continuous decline in the capacity in the next 10 cycles are observed. The capacity decreases to 14 mAh g^{-1} after 10 cycles, indicating Li_2TiO_3 might be electrochemical inactive or its reversible capacity is quite trivial. Thirdly, the relatively low coulombic efficiency during the first 10 cycles suggests an irreversible Li^+ ion insertion and extraction process. The cyclic voltammetry profiles at scan rates of 0.1 mV s^{-1}, 0.2 mV s^{-1}, 0.3 mV s^{-1}, 0.4 mV s^{-1}, 1.0 mV s^{-1}, and 2.0 mV s^{-1} (shown in Fig. 2(c)) illustrate that there are one couple of reduction and oxidation peaks at about 1.54 V and 1.6 V which are assigned to the insertion and extraction of Li^+ ions contributed by a trait of $Li_4Ti_5O_{12}$. Besides the reduction/oxidation peaks, capacitive plateaus at lower potential are also found during the scans. These peeks are broad and quite similar to that of $Ni(OH)_2$ and V_2O_5/polyaniline layer by layer electrodes, demonstrating that both faradic reaction and double layer capacitance are involved in the electrochemical process [40,41]. A line plotted with log *I* and log *V* on the basis of these peak points is shown in Fig. 2(d). The slope of the line for Li_2TiO_3 is 0.8, which further demonstrates the existence of pseudocapacitive effect in the discharge and charge processes [42].

3.2. Structure and morphology characterization of $Li_4Ti_5O_{12}/Li_2TiO_3$ composites

The crystalline structure of $Li_4Ti_5O_{12}/Li_2TiO_3$ composites, $Li_4Ti_5O_{12}/TiO_2$ composites and pristine $Li_4Ti_5O_{12}$ revealed by XRD diffraction patterns is given in Fig. 3. Peaks at 2θ of 18.3°, 35.6°, 43.2°, 57.2°, and 62.9° detected in all patterns well match the diffraction peaks of spinel $Li_4Ti_5O_{12}$ listed in the ICDD/JCPDS file numbered 49-0207. Besides the typical diffraction peaks of spinel

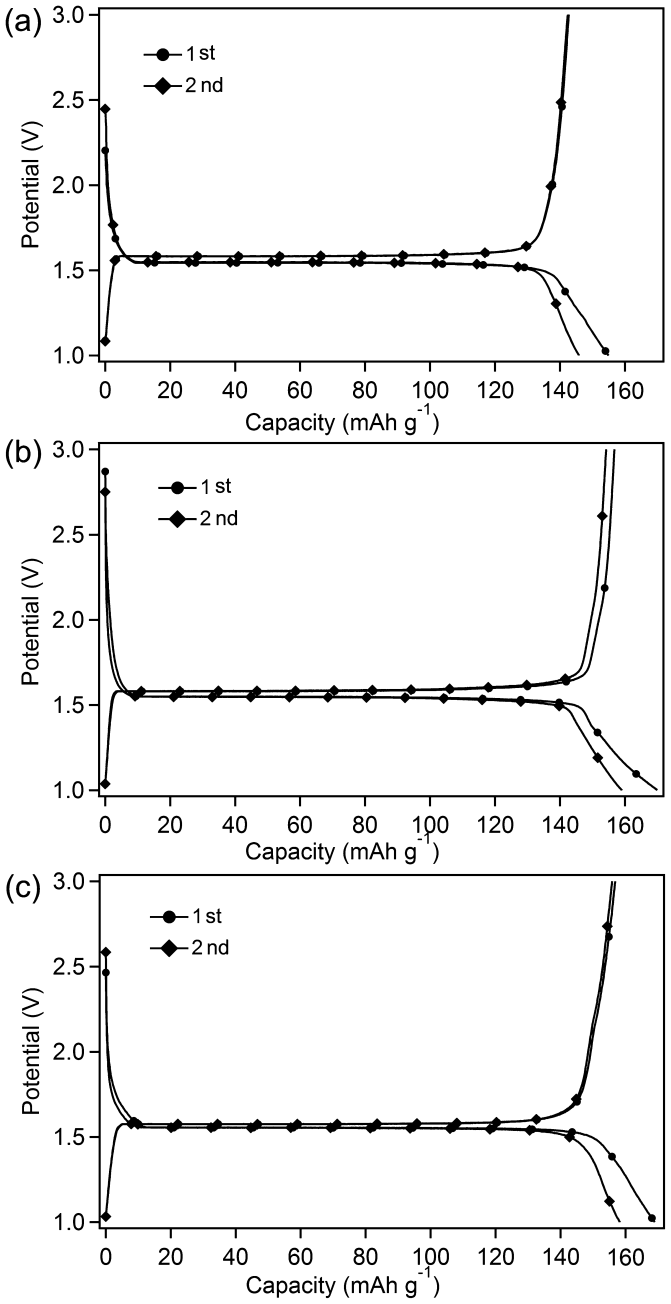

Fig. 5. The first two discharge–charge curves of (a) $Li_4Ti_5O_{12}/Li_2TiO_3$ composite L2 (b) pure $Li_4Ti_5O_{12}$ (c) $Li_4Ti_5O_{12}/TiO_2$ material T1.

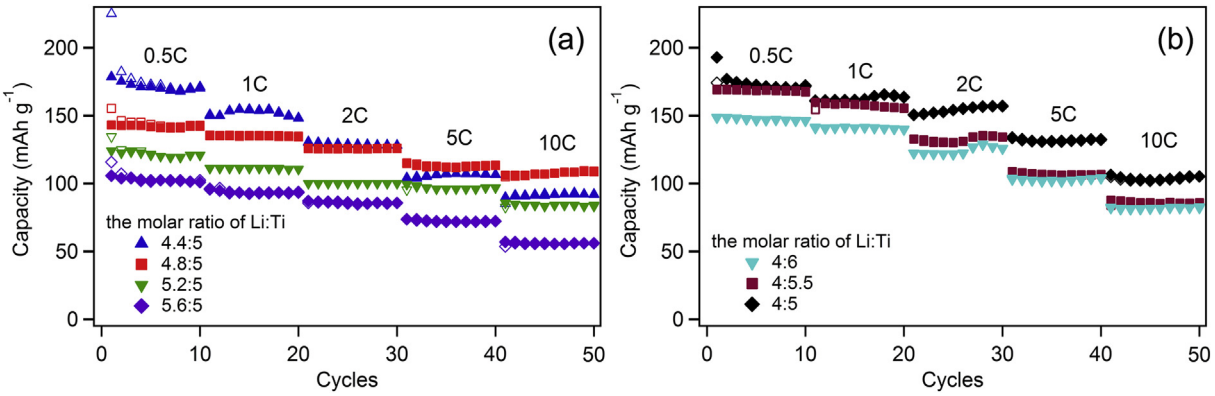

Fig. 6. The rate performance of the samples with different molar ratios of Li:Ti. (a) $Li_4Ti_5O_{12}/Li_2TiO_3$ composites (L1 – 4.4:5, L2 – 4.8:5, L3 – 5.2:5, L4 – 5.6:5) (b) $Li_4Ti_5O_{12}/TiO_2$ composites (T2 – 4:6, T1 – 4:5.5, T0 – 4:5).

$Li_4Ti_5O_{12}$, the peaks at 18.4°, 35.7°, 43.3°, 57.6°, 62.8°, and 66.4° are also detected in $Li_4Ti_5O_{12}/Li_2TiO_3$ composite (shown in Fig. 3(a)), which can be assigned to Li_2TiO_3. The weight ratio of impure Li_2TiO_3 phase increases with the increment of Li:Ti ratio and is calculated to be 5.0 wt%, 14.5 wt%, 23.5 wt% and 31.9 wt% for sample L1 (4.4:5), L2 (4.8:5), L3 (5.2:5), and L4 (5.6:5), respectively. For $Li_4Ti_5O_{12}/TiO_2$ composites (shown in Fig. 3(b)), anatase TiO_2 (PDF#21-1272) and rutile TiO_2 (PDF#21-1276) coexist in the dual-phase system. The presentation of rutile TiO_2 is owed to relatively lower sintering temperature or shorter calcination time employed in the synthesis process, which is in accord with the tendency observed by Yoon and the coworkers [43]. The weight percentage of TiO_2 impurity was reduced with increasing Li:Ti ratio.

The morphology information of $Li_4Ti_5O_{12}/Li_2TiO_3$ composite L2, pure $Li_4Ti_5O_{12}$, and $Li_4Ti_5O_{12}/TiO_2$ composite T1 is provided in Fig. 4. All the particles are submicron-sized and quasi-spherical, suggesting these three samples are very alike. The tap densities of $Li_4Ti_5O_{12}/Li_2TiO_3$ composite L2, pure $Li_4Ti_5O_{12}$, and $Li_4Ti_5O_{12}/TiO_2$ composite T1 are 0.79 g cm^{-1}, 0.82 g cm^{-1}, and 0.79 g cm^{-1}, which further confirms that there is no obvious difference considering the particle size distribution and surface morphology.

3.3. *The electrochemical performance of $Li_4Ti_5O_{12}/Li_2TiO_3$ composites*

Galvanostatic discharge–charge tests were done to investigate cycling stability and rate performance. There is no evident difference in the shapes of the first two cycles of the batteries made of samples L2, L0 and T1 (shown in Fig. 5). The coulombic efficiency in the first cycle of the batteries assembled with $Li_4Ti_5O_{12}/Li_2TiO_3$ composite L2 is 95%, slightly higher than that of pure $Li_4Ti_5O_{12}$ (92%) and $Li_4Ti_5O_{12}/TiO_2$ composite T1 (93%). Rate performance of the as-prepared samples is shown in Fig. 6. The average initial capacities are 149 mAh g^{-1}, 169 mAh g^{-1}, 174 mAh g^{-1}, 170 mAh g^{-1}, 175 mAh g^{-1}, 155 mAh g^{-1}, 124 mAh g^{-1}, and 105 mAh g^{-1} for Li:Ti of 4:6, 4:5.5, 4:5, 4.2:5, 4.4:5, 4.8:5, 5.2:5 and 5.6:5 at a discharge–charge rate of 0.5 C. Apparently, the initial discharge capacity of the $Li_4Ti_5O_{12}/Li_2TiO_3$ composites decreased while the Li:Ti molar ratio was promoted (shown in Fig. 6(a)). As a contrast, the initial capacity of the $Li_4Ti_5O_{12}/TiO_2$ composites was elevated by increasing Li:Ti ratio (shown in Fig. 6(b)). In order to highlight the difference among the typical composites, the rate performances of $Li_4Ti_5O_{12}/Li_2TiO_3$ composite L2, $Li_4Ti_5O_{12}/TiO_2$ composite T1 and $Li_4Ti_5O_{12}$ are plotted in Fig. 7. The lower initial capacity of $Li_4Ti_5O_{12}/Li_2TiO_3$ composites can be attributed to the poor reversible capacity of Li_2TiO_3, which is only 14 mAh g^{-1} after 10 cycles. Although the initial capacity is lower, $Li_4Ti_5O_{12}/Li_2TiO_3$ composite L2 synthesized with the molar ratio Li:Ti of 4.8:5 exhibits the best rate capability. The capacity of 108 mAh g^{-1} is achieved at the highest rate of 10 C for $Li_4Ti_5O_{12}/Li_2TiO_3$ composite L2, which is significantly over than 85 mAh g^{-1} and 60 mAh g^{-1} of $Li_4Ti_5O_{12}/TiO_2$ composite T1 and pristine $Li_4Ti_5O_{12}$.

The cycling performances of the as-prepared $Li_4Ti_5O_{12}/Li_2TiO_3$ composite L2, $Li_4Ti_5O_{12}/TiO_2$ composite T1, and pristine $Li_4Ti_5O_{12}$

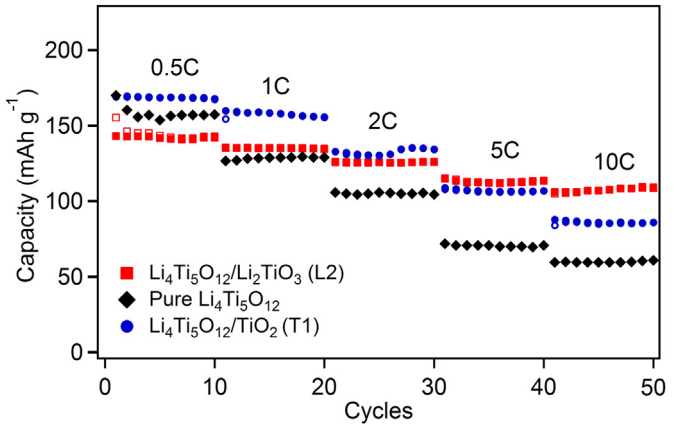

Fig. 7. The comparison of the rate performances of the batteries prepared by $Li_4Ti_5O_{12}/Li_2TiO_3$ composite L2, $Li_4Ti_5O_{12}/TiO_2$ composite T1 and pure $Li_4Ti_5O_{12}$.

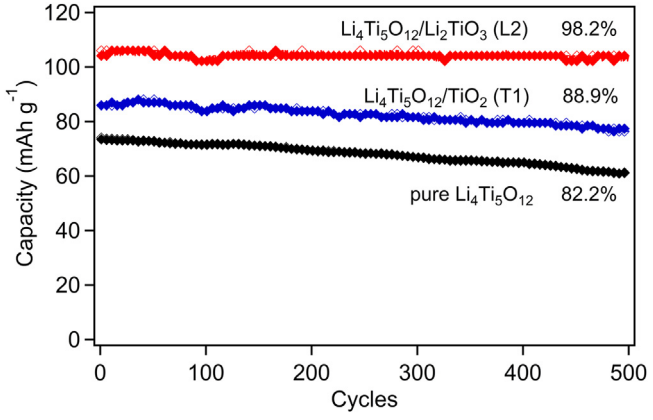

Fig. 8. The cycle performances at the discharge–charge rate of 10 C of the batteries prepared by $Li_4Ti_5O_{12}/Li_2TiO_3$ composite L2, $Li_4Ti_5O_{12}/TiO_2$ composite T1 and pure $Li_4Ti_5O_{12}$.

are presented in Fig. 8. After 500 cycles at the discharge–charge rate of 10 C, the capacity retention was kept at a high level of 98.2%, which is much higher than that of $Li_4Ti_5O_{12}$ (82.2%) and $Li_4Ti_5O_{12}$/TiO_2 (88.9%). This result is also better than previous reports on carbon-coated and cation doped $Li_4Ti_5O_{12}$ [14,18,20,22]. Yang and his coworkers [44] have reported that $Li_4Ti_5O_{12}$ tends to suffer from phase transformation at the outmost surface when soaked in electrolyte, where Li^+ and O^{2-} ions are taken away from the surface of $Li_4Ti_5O_{12}$ particles during the interfacial reaction between $Li_4Ti_5O_{12}$ and electrolyte, resulting in the formation of anatase TiO_2. Herein, Li_2TiO_3 with Li-rich structure might be helpful to stabilize the crystal structure of $Li_4Ti_5O_{12}$. In fact, Li_2TiO_3 has been successfully applied to improve cyclic performance of $LiMO_2$ (M = Ni, Co, Mn), $LiMn_{0.5}Ni_{0.5}O_2$, $LiFeO_2$, which could effectively protect the active materials from reacting with the electrolytes [39,45,46].

The cyclic voltammograms of the as-prepared $Li_4Ti_5O_{12}/Li_2TiO_3$ composite L2, $Li_4Ti_5O_{12}/TiO_2$ composite T1 and pristine $Li_4Ti_5O_{12}$ materials are shown in Fig. 9. All the plots have one couple of reduction and oxidation peaks reflecting Li^+ ion insertion into and extraction from the active materials separately. There are no characteristic redox peaks associated with Li_2TiO_3 or TiO_2, which agree with the galvanostatic discharge–charge results, showing potential plateaus for discharge–discharge processes. Although the XRD measurements confirm the existence of Li_2TiO_3 or TiO_2 impurity, electrochemical tests do not detect their corresponding contribution. It indicates that the amount of the impurity might be not high enough for electrochemical characterization. At the scan rate of 0.1 mV s^{-1}, the reduction peaks of $Li_4Ti_5O_{12}/Li_2TiO_3$ composite L2, $Li_4Ti_5O_{12}/TiO_2$ composite T1, and pristine $Li_4Ti_5O_{12}$ locate at 1.45 V, 1.46 V, and 1.42 V, respectively. The corresponding oxidation peaks are positioned at 1.66 V, 1.68 V, and 1.77 V. No evident polarization is detected for all the samples at slow scan rate. The two peaks move toward the opposite direction with the elevated scan rate, which means that the electrochemical polarization becomes larger and larger. The smallest polarization of $Li_4Ti_5O_{12}/Li_2TiO_3$ composite L2 at high current rate enables the improvement of the rate performance possible.

To further understand why the rate performance of $Li_4Ti_5O_{12}$/Li_2TiO_3 composite is better than that of $Li_4Ti_5O_{12}/TiO_2$ composite T1 and pristine $Li_4Ti_5O_{12}$, the ion conductivities are evaluated. Fig. 10(a) shows the impedance spectra of these three bulk platelets. The corresponding equivalent circuit is demonstrated as an insert. The intercept of the depressed semicircle on the *X* axis is the resistance of the prepared platelets. The resistances fitted from the equivalent circuit are 0.4 MΩ, 1.2 MΩ, 1.6 MΩ, and 3.3 MΩ for $Li_4Ti_5O_{12}/Li_2TiO_3$ composite L2, pristine $Li_4Ti_5O_{12}$, $Li_4Ti_5O_{12}/TiO_2$ composite T1, and pristine Li_2TiO_3 in sequence. The calculated intrinsic ionic conductivity of $Li_4Ti_5O_{12}/Li_2TiO_3$ composite L2 (1.7×10^{-6} S cm^{-1}) is much higher than those of pristine $Li_4Ti_5O_{12}$ (5.7×10^{-7} S cm^{-1}), pristine Li_2TiO_3 (2.5×10^{-7} S cm^{-1}), and $Li_4Ti_5O_{12}/TiO_2$ composite T1 (4.2×10^{-7} S cm^{-1}). It can be concluded that Li-rich grain boundaries with high concentration of diffusion-mediating defects make fast diffusivity possible.

Fig. 10(b) exhibits the Nyquist plots of the batteries with $Li_4Ti_5O_{12}/Li_2TiO_3$ composite L2, $Li_4Ti_5O_{12}/TiO_2$ composite T1 and pristine $Li_4Ti_5O_{12}$ as working electrodes. All the plots possess a depressed semicircle at high to intermediate frequency and an oblique line at low frequency. As shown in the insert of Fig. 10(b), the semicircle, which is associated with the charge-transfer resistance (*R*ct) and a double layer capacitance at the interface between the active material and the electrolyte, is represented by *R*ct and CPE (a constant phase element), separately. The oblique line corresponding to *W* (Warburg impedance) reflects the diffusion of Li^+ in the bulk phase of the active material. *R*s is the resistance of the electrical contacts, separator and electrolyte [47]. The charge-

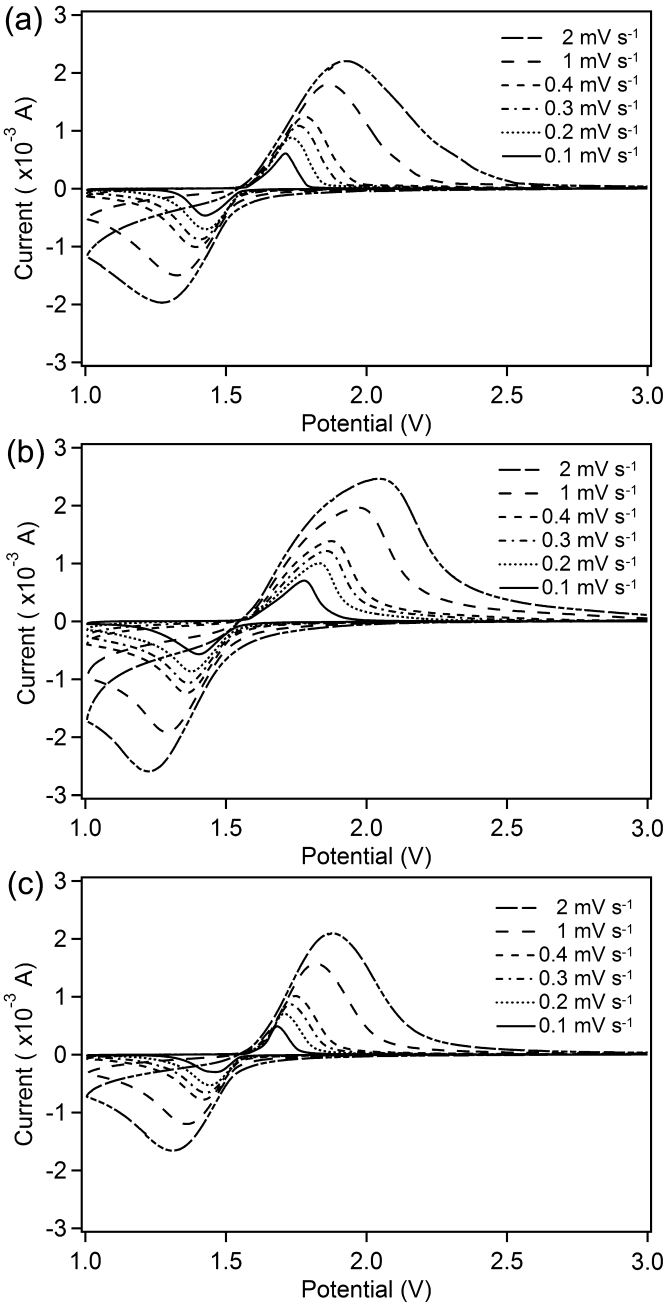

Fig. 9. The cyclic voltammograms of the batteries prepared by (a) $Li_4Ti_5O_{12}/TiO_2$ composite T1 (b) pure $Li_4Ti_5O_{12}$ (c) $Li_4Ti_5O_{12}/Li_2TiO_3$ composite L2.

transfer resistances of $Li_4Ti_5O_{12}/Li_2TiO_3$ composite L2 (76.9 Ω) and $Li_4Ti_5O_{12}/TiO_2$ composite T1 (146.5 Ω) are much smaller than that of pure $Li_4Ti_5O_{12}$ (178.6 Ω), which means that the charge-transfer process is much easier at the interface of electrolyte/particles for the composites. Combined with the higher ionic conductivity, it is reasonable for $Li_4Ti_5O_{12}/Li_2TiO_3$ composite L2 to exhibit a good rate performance.

4. Conclusions

In this work, submicron-sized $Li_4Ti_5O_{12}/Li_2TiO_3$ composites with Li-rich grain boundaries were successfully synthesized by a simple, mass production preferred solid state process. $Li_4Ti_5O_{12}/TiO_2$ composites and pristine $Li_4Ti_5O_{12}$ and Li_2TiO_3 were synthesized

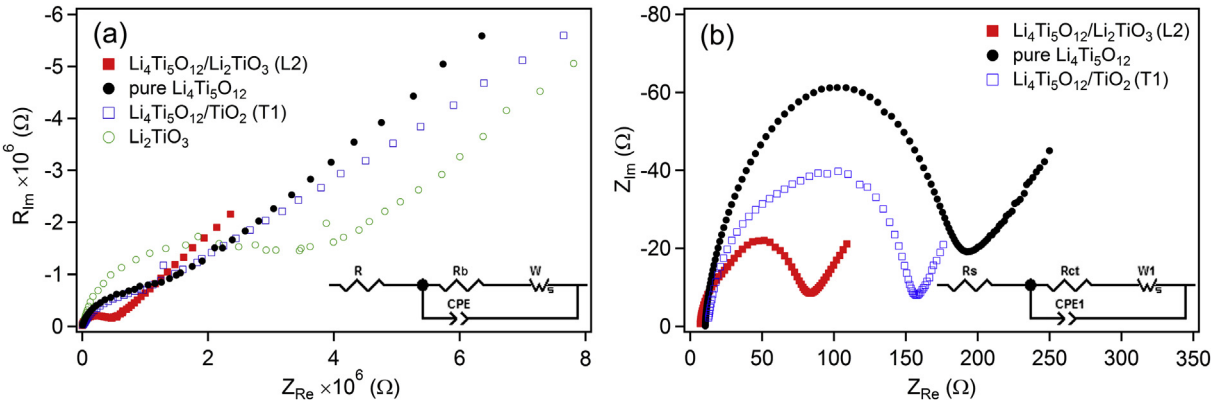

Fig. 10. EIS and equivalent circuits of (a) the as-prepared platelets (b) the batteries prepared by $Li_4Ti_5O_{12}/Li_2TiO_3$ composite L2, $Li_4Ti_5O_{12}/TiO_2$ composite T1 and pure $Li_4Ti_5O_{12}$.

similarly for comparison. Even though the particle size and crystallinity were quite alike for $Li_4Ti_5O_{12}$ based materials, the cycle stability and rate capability of $Li_4Ti_5O_{12}/Li_2TiO_3$ composites were much better than those of $Li_4Ti_5O_{12}/TiO_2$ composites and pristine $Li_4Ti_5O_{12}$. The higher ionic conductivity of the $Li_4Ti_5O_{12}/Li_2TiO_3$ powders and the smaller charge-transfer resistance at the electrolyte/particle interface were the main reasons for the improved rate performance. Furthermore, the $Li_4Ti_5O_{12}/Li_2TiO_3$ composites demonstrated the improved cycle performance even at high current rate of 10 C, where Li_2TiO_3 was supposed to promote the structure stability of $Li_4Ti_5O_{12}$ active material in the electrolyte.

Acknowledgments

This work was supported by NSFC, China (_501100001809) (Grant nos: 21073029, 11234013, 51211140045), RFDP (no. 20100185110019), Program for New Century Excellent Talents in University (no. NCET-10-0296), Fundamental Research Funds for the Central Universities (nos. ZYGX2012Z003, 103.1.2 E022050205).

References

[1] Z. Yang, J. Zhang, M.C.W. Kintner-Meyer, X. Lu, D. Choi, J.P. Lemmon, J. Liu, Chem. Rev. 115 (2011) 3577–3613.
[2] B. Kang, G. Ceder, Nature 458 (2009) 190–193.
[3] Y.K. Sun, S.T. Myung, B.C. Park, J. Prakash, I. Belharouak, K. Amine, Nat. Mater. 8 (2009) 320–324.
[4] B. Dunn, H. Kamath, J.M. Tarascon, Science 334 (2011) 928–935.
[5] N. Kamaya, K. Homma, Y. Yamakawa, M. Hirayama, R. Kanno, M. Yonemura, T. Kamiyama, Y. Kato, S. Hama, K. Kawamoto, Nat. Mater. 10 (2011) 682–686.
[6] Z.Y. Wen, J.Z. Li, J. Inorg. Mater. 28 (2013) 1163–1164.
[7] F. Orsini, A. Du Pasquier, B. Beaudouin, J. Tarascon, M. Trentin, N. Langenhuizen, E. De Beer, P. Notten, J. Power Sources 81 (1999) 918–921.
[8] J.W. Li, A.J. Zhou, X.Q. Liu, J.Z. Li, J. Inorg. Mater. 28 (2013) 1207–1212.
[9] T. Ohzuku, A. Ueda, N. Yamamoto, J. Electrochem. Soc. 142 (1995) 1431–1435.
[10] K. Zaghib, M. Simoneau, M. Armand, M. Gauthier, J. Power Sources 81 (1999) 300–305.
[11] A. Guerfi, S. Sevigny, M. Lagace, P. Hovington, K. Kinoshita, K. Zaghib, J. Power Sources 119 (2003) 88–94.
[12] C. Chen, J. Vaughey, A. Jansen, D. Dees, A. Kahaian, T. Goacher, M. Thackeray, J. Electrochem. Soc. 148 (2001) A102–A104.
[13] T.F. Yi, Y. Xie, J. Shu, Z. Wang, C.B. Yue, R.S. Zhu, H.B. Qiao, J. Electrochem. Soc. 158 (2011) A266–A274.
[14] Y.-R. Jhan, C.-Y. Lin, J.-G. Duh, Mater. Lett. 65 (2011) 2502–2505.
[15] Z. Wang, G. Chen, J. Xu, Z. Lv, W. Yang, J. Phys. Chem. Solids 72 (2011) 773–778.
[16] T.F. Yi, J. Shu, Y.R. Zhu, X.D. Zhu, C.B. Yue, A.N. Zhou, R.S. Zhu, Electrochim. Acta 54 (2009) 7464–7470.
[17] Y.H. Yin, S.Y. Li, Z.J. Fan, X.L. Ding, S.T. Yang, Mater. Chem. Phys. 130 (2011) 186–190.
[18] Y. Wang, W. Zou, X.Y. Dai, L.D. Feng, H.Q. Zhang, A.J. Zhou, J.Z. Li, Ionics (2014), http://dx.doi.org/10.1007/s11581-014-1103-6.
[19] T. Yuan, R. Cai, Z. Shao, J. Phys. Chem. C 115 (2011) 4943–4952.
[20] L. Zhao, Y.S. Hu, H. Li, Z. Wang, L. Chen, Adv. Mater. 23 (2011) 1385–1388.
[21] H. Pan, L. Zhao, Y.S. Hu, H. Li, L. Chen, Chemsuschem 5 (2011) 526–529.
[22] H.Q. Zhang, Q.J. Deng, C.X. Mou, Z.L. Huang, Y. Wang, A.J. Zhou, J.Z. Li, J. Power Sources 239 (2013) 538–545.
[23] E. Matsui, Y. Abe, M. Senna, A. Guerfi, K. Zaghib, J. Am. Ceram. Soc. 91 (2008) 1522–1527.
[24] J. Lim, E. Choi, V. Mathew, D. Kim, D. Ahn, J. Gim, S.H. Kang, J. Kim, J. Electrochem. Soc. 158 (2011) A275–A280.
[25] J.-G. Kim, D. Shi, M.-S. Park, G. Jeong, Y.-U. Heo, M. Seo, Y.-J. Kim, J.H. Kim, S.X. Dou, Nano Res. 6 (2013) 365–372.
[26] S. Huang, Z. Wen, J. Zhang, X. Yang, Electrochim. Acta 52 (2007) 3704–3708.
[27] S. Huang, Z. Wen, J. Zhang, Z. Gu, X. Xu, Solid State Ionics 177 (2006) 851–855.
[28] S. Huang, Z. Wen, X. Zhu, Z. Gu, Electrochem. Commun. 6 (2004) 1093–1097.
[29] C.C. Li, Q.H. Li, L.B. Chen, T.H. Wang, ACS Appl. Mater. Interfaces 4 (2012) 1233–1238.
[30] M. Marinaro, F. Nobili, R. Tossici, R. Marassi, Electrochim. Acta 89 (2013) 555–560.
[31] S. Huang, Z. Wen, B. Lin, J. Han, X. Xu, J. Alloys Compd. 457 (2008) 400–403.
[32] J. Shu, L. Hou, R. Ma, M. Shui, L. Shao, D. Wang, Y. Ren, W. Zheng, RSC Adv. 2 (2012) 10306–10309.
[33] X. Li, C. Lai, C. Xiao, X. Gao, Electrochim. Acta 56 (2011) 9152–9158.
[34] M.M. Rahman, J.Z. Wang, M.F. Hassan, D. Wexler, H.K. Liu, Adv. Energy Mater. 1 (2011) 212–220.
[35] Y.Q. Wang, L. Gu, Y.G. Guo, H. Li, X. He, S. Tsukimoto, Y. Ikuhara, L. Wan, J. Am. Chem. Soc. 134 (2012) 7874–7879.
[36] H. Kleykamp, Fusion Eng. Des. 61 (2002) 361–366.
[37] M. Mohammadi, D. Fray, J. Sol-Gel Sci. Technol. 55 (2010) 19–35.
[38] M. Tabuchi, A. Nakashima, H. Shigemura, K. Ado, H. Kobayashi, H. Sakaebe, K. Tatsumi, H. Kageyama, T. Nakamura, R. Kanno, J. Mater. Chem. 13 (2003) 1747–1757.
[39] J. Morales, J. Santos-Peña, R. Trócoli, S. Franger, J. Nanoparticle Res. 10 (2008) 217–226.
[40] L. Shao, J.W. Jeon, J.L. Lutkenhaus, Chem. Mater. 24 (2012) 181–189.
[41] J. Liu, C. Cheng, W. Zhou, H. Li, H.J. Fan, Chem. Commun. 47 (2011) 3436–3438.
[42] A.J. Bard, L.R. Faulkner, Electrochemical Methods: Fundamentals and Applications, Wiley & Sons, Inc., New York, 2001, pp. 226–260.
[43] J.W. Shin, C.H. Hong, D.H. Yoon, J. Am. Ceram. Soc. 95 (2012) 1894–1900.
[44] Y.-B. He, B. Li, M. Liu, C. Zhang, W. Lv, C. Yang, J. Li, H. Du, B. Zhang, Q.-H. Yang, J.-K. Kim, F. Kang, Sci. Reports 2 (2012).
[45] J. Lu, Q. Peng, W. Wang, C. Nan, L. Li, Y. Li, J. Am. Chem. Soc. 135 (2013) 1649–1652.
[46] J.S. Kim, C. Johnson, M. Thackeray, Electrochem. Commun. 4 (2002) 205–209.
[47] G.T.K. Fey, C.Z. Lu, T.P. Kumar, J. Power Sources 115 (2003) 332–345.